Chemical Science

Acid/Base-Regulated Reversible Electron Transfer Disproportionation of N-N linked Bicarbazole and Biacridine Derivatives

Journal:	*Chemical Science*
Manuscript ID:	SC-EDG-03-2015-000946.R1
Article Type:	Edge Article
Date Submitted by the Author:	15-Apr-2015

Complete List of Authors:	Pandit, Palash; Institute for Molecular Science, Yamamoto, Koji; Institute for Molecular Science, Nakamura, Toshikazu; Institute for Molecular Science, Nishimura, Katsuyuki; Institute for Molecular Science, Kurashige, Yuki; Institute for Molecular Science, Yanai, Takeshi; Institute for Molecular Science, Nakamura, Go; Institute for Molecular Science, Masaoka, Shigeyuki; Institute for Molecular Science, Furukawa, Ko; Niigata University, Yakiyama, Yumi; Pohang University of Science and Technology, Division of Advanced Materials Science Kawano, Masaki; POSTECH, Advanced Materials Science Higashibayashi, Shuhei; Institute for Molecular Science,

Journal Name

RSCPublishing

ARTICLE

Acid/Base-Regulated Reversible Electron Transfer Disproportionation of N-N linked Bicarbazole and Biacridine Derivatives

Cite this: DOI: 10.1039/x0xx00000x

Received 00th January 2012,
Accepted 00th January 2012

DOI: 10.1039/x0xx00000x

www.rsc.org/

Palash Pandit,[‡a] Koji Yamamoto,[‡a] Toshikazu Nakamura,[ab] Katsuyuki Nishimura,[ab] Yuki Kurashige,[abc] Takeshi Yanai,[ab] Go Nakamura,[ab] Shigeyuki Masaoka,[ab] Ko Furukawa,[d] Yumi Yakiyama,[e] Masaki Kawano[e] and Shuhei Higashibayashi*[abf]

Regulation of the electron transfer on organic substances by external stimuli is a fundamental issue in science and technology such as organic materials, chemical synthesis, and biological metabolism. Nevertheless, acid/base-responsive organic materials with reversible electron transfer have not been well studied and developed owing to the difficulty to invent a mechanism to associate acid/base stimuli and electron transfer. We discovered a new phenomenon that N-N linked bicarbazole (BC) and tetramethylbiacridine (TBA) derivatives undergo electron transfer disproportionation by acid stimulus, giving their stable radical cations and reduced species. The reaction goes through a biradical intermediate generated by the acid-triggered N-N bond cleavage reaction of BC or TBA, which acts as a two electron acceptor to undergo electron transfer reactions with two equivalents of BC or TBA. In addition, the disproportionation reaction is highly reversible by neutralization with NEt_3 in case of TBA, recovering TBA through the back electron transfer and N-N bond formation reactions. This highly reversible electron transfer reaction is possible due to the association between acid stimulus and electron transfer with the acid-regulated N-N bond cleavage/formation reactions as an efficient switching mechanism, the multi-electron redox property as both donor and acceptor, the extraordinary stability of the radical species, the high-selective reactivity, and the balance of the redox potentials. This discovery provides new design concepts for acid/base-regulated organic electron transfer systems, chemical reagents, or organic materials.

Introduction

Regulation of the electron transfer redox process on organic substances by external stimuli (light, electric field, pressure, pH, chemicals, etc.) is a fundamental issue in both science and technology such as in organic materials, chemical synthesis, and biological metabolism.[1] Development of redox-active organic compounds and assembled systems with a responsive function to external stimuli leads to wide applications. Among the external stimuli, the control of the electron transfer redox reaction on organic substances by light or electric field has been extensively studied and developed for organic materials/devices and chemical syntheses.[1a,2] Light or electric field directly induce the electron transfer redox reaction followed by the responsive function. In contrast, it is more difficult to design and develop redox-active organic compounds responsive to stimuli such as an acid/base[3-5] or other chemicals[6,7], because these stimuli do not directly induce electron transfer or redox conversion but protonation, complexation, or adsorption. Thus, it is necessary to connect the chemical or physical changes to the electron transfer or redox transformation followed by the responsive function for regulation by these stimuli. Another important factor is the reversibility or the repeatability of the reaction and the responsiveness of the system for sustainability, which requires either the redox reaction process to be reversible by the opposite stimuli (e.g., neutralization) or the responsive material to be a catalyst repeating a redox reaction. These requirements make the development of acid/base-responsive organic materials with multi-functional properties very difficult. Although many acid-responsive organic compounds including pH indicators have been developed,[8] acids regulate non-redox processes such as isomerization, complexation, or conformational change followed by the responsive function. Only tetrathiafulvalene (TTF)[3] and 2,2,6,6-tetramethyl-1-piperidinyloxyl (TEMPO)[4] among artificial organic compounds have been reported to show an acid-responsive reversible electron transfer reaction through disproportionation owing to their excellent redox properties (Scheme S1).[5] However, the reaction is very low yielding (~1%) or requires very strong acids (conc. H_2SO_4) due to the simple protonation and

subsequent electron transfer mechanism. To realize a more efficient acid-responsive electron transfer system, a sophisticated function to associate the acid/base stimuli with an electron transfer reaction is necessary. As examples of other chemical stimuli, metal ion-promoted[6] or anion-mediated[7] electron transfer of donor-acceptor type TTF derivatives have been reported, utilizing conformational change or supramolecular assembly induced by metal ion or anion complexations as the efficient switching mechanism.

During a course of our study on N-N linked 1,1',9,9'-bicarbazole (BC) and 9,9,9',9'-tetramethyl-4,4',10,10'-biacridine (TBA) derivatives (Fig. 1), we encountered an unexpected phenomenon that their ^{1}H NMR spectra in $CDCl_3$ indicated extremely broad signals, which turned out to be due to acid-responsive generation of unknown radical species. The unknown radical species generated by addition of acids in organic solvents were highly stable under air at room temperature in the acidic conditions. Furthermore, to our surprise, BC or TBA was recovered in high yields by neutralization with NEt_3. After thorough experimental investigations and computational studies, this phenomenon was fully elucidated to be acid-responsive electron transfer disproportionation to give their stable radical cations and reduced species (Scheme 1). These compounds exhibit a contrast change of photophysical and magnetic properties before and after the reaction. The reaction goes through a biradical intermediate generated by the acid-triggered N-N bond cleavage reaction of BC or TBA, which acts as a two electron acceptor to undergo electron transfer reactions with two equivalents of BC or TBA to produce the radical cations and reduced species. This electron transfer disproportionation reaction is possible due to the association between acid stimulus and electron transfer with the acid-triggered N-N bond cleavage reaction, the multi-electron redox property as both donor and acceptor, the extraordinary stability of the radical

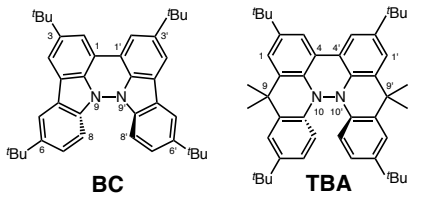

Fig.1 1,1',9,9'-Bicarbazole (BC) and tetramethyl-4,4',10,10'-biaciridine (TBA) derivatives with ^{t}Bu substituents.

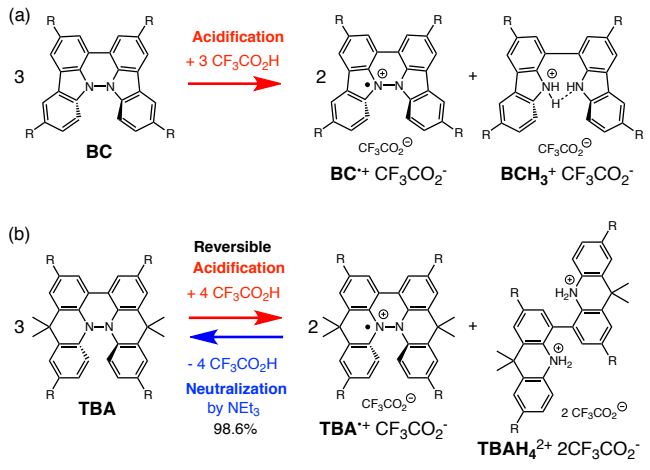

Scheme 1 Acid/base-regulated electron transfer disproportionation of (a) BC and (b) TBA

species, and the high-selective reactivity. While BC and TBA exhibited the similar disproportionation reactions, several differences were admitted and a most notable difference is the reversibility of reaction. The disproportionation reaction in TBA was found to be highly reversible by neutralization with NEt_3, recovering TBA through the back electron transfer and N-N bond formation reactions. This high reversibility was realized by the acid-regulated N-N bond cleavage/formation reactions as an efficient switching mechanism and the balance of the redox potentials of involved chemical species. Here, we report the full identification of these compounds, phenomenon, and its mechanism by thorough experimental investigation and theoretical calculations.

Result and discussion

Synthesis

Several synthetic pathways for 1,1',9,9'-bicarbazole (BC) with *t*-Bu groups were developed from 3,6-di-*t*-butylcarbazole **1** (Scheme 2). Bromocabazole **2**, prepared from **1**, was converted to the dimer **3** through the oxidative coupling between nitrogen atoms by $KMnO_4$[9] in acetone in 75% yield. $Ni(COD)_2$-mediated reductive coupling of **3** afforded the desired BC in 69% yield. In another pathway, dimer **4** was obtained from **2** by the $Ni(COD)_2$-mediated reductive coupling in 87% yield. Dimer **4** was also synthesized through the direct oxidative coupling of carbazole **1** using $FeCl_3$ in 41% yield. Oxidative coupling of **4** between nitrogen atoms using Bu_4NMnO_4 in pyridine afforded BC in 65% yield. Tetramethyl-4,4',10,10'-biacridine (TBA) was synthesized from 2,7-di-*tert*-butyl-9,10-dihydro-9,9-dimethylacridine **5** (Scheme 3). Bromoacridine **6** obtained from **5** by bromination was converted to the dimer **7** by the $Ni(COD)_2$-mediated reductive coupling in 95% yield. Oxidative coupling of **7** using Bu_4NMnO_4 in pyridine afforded TBA in 86% yield.

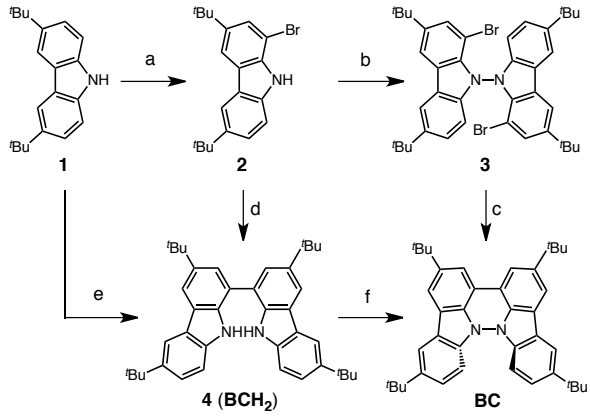

Scheme 2 Synthesis of bicarbazole (BC). Reagents and conditions: (a) *N*-bromosuccinimide 110 mol%, SiO_2, CH_2Cl_2, rt, 4 h, 86%; (b) $KMnO_4$ 250 mol%, acetone, 60 °C, 4 h, 75%; (c) $Ni(COD)_2$ 150 mol%, COD 150 mol%, 2,2'-bipyridyl 150 mol%, THF, 45 °C, 6 h, 69%; (d) $Ni(COD)_2$ 300 mol%, COD 300 mol%, 2,2'-bipyridyl 300 mol%, THF, 80 °C, 6 h, 87%; (e) $FeCl_3$ 200 mol%, CH_2Cl_2, rt, 15 min, 41%; (f) Bu_4NMnO_4 200 mol%, pyridine, 70 °C, 24 h, 65%.

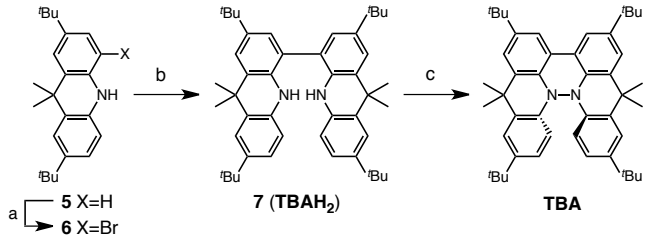

Scheme 3 Synthesis of tetramethylbiacridine (TBA). Reagents and conditions: (a) *N*-bromosuccinimide 103 mol%, $CHCl_3$, 60 °C, 1 h, 57%; (b) $Ni(COD)_2$ 300 mol%, COD 300 mol%, 2,2'-bipyridyl 300 mol%, THF, 80 °C, 6 h, 95%; (c) Bu_4NMnO_4 250 mol%, pyridine, rt, 12 h, 86%.

Disproportionation of 1,1',9,9'-bicarbazole (BC).

The X-ray crystallographic analysis showed a characteristic helical molecular shape of BC with the dihedral angle $\angle C_{8a}N_9N_{9'}C_{8a'}$=48 ° due to the steric repulsion between C and C' rings (C_8-$C_{8'}$ distance=3.33 Å)(Fig. 2). The color of the solution of BC in CH_2Cl_2 was yellow and the UV-Vis-NIR absorption spectrum showed absorption at 461 nm (Fig. 3a, c). BC exhibited strong green fluorescence with the emission maximum at 522 nm in CH_2Cl_2 (Fig. 3b, e) and the quantum yield was determined to be 69%. While the structure of BC was unambiguously determined by X-ray crystallographic analysis, the ^1H NMR spectrum in $CDCl_3$ indicated extremely broad signals (Electronic Supplementary Information). In contrast, the solid state ^{13}C, ^1H, and ^{15}N NMR spectra of BC showed the expected signals associated with the structure (Table S1, Fig. S1-S4). In order to reveal this unexpected phenomenon, we investigated the effects of potential factors such as light, air, and solvent, and the origin of the broadening turned out to be the effect of contaminant hydrochloric acid in $CDCl_3$. Thus, we examined the effects of acids on the physical properties of BC. When the solution of BC in CH_2Cl_2 was treated by CF_3CO_2H (TFA) at room temperature under either aerobic or anaerobic conditions, the color of the solution drastically changed from yellow to deep indigo-blue (Fig. 3d). In the UV-Vis-NIR spectra in CH_2Cl_2, the absorption of BC at 461 nm was decreased by the addition of CF_3CO_2H and new broad absorptions at 540 and 635 nm appeared in the visible to near infrared light region (Fig. 3a). The new absorption bands were increased by the addition of more CF_3CO_2H, and they were nearly saturated by the addition of 500 mol% CF_3CO_2H. In accordance with the absorption spectral change, the emission of BC also disappeared after the addition of CF_3CO_2H. Similar changes in the appearance and absorption spectra were also observed in other organic solvents ($CHCl_3$, 1,2-dichloroethane, benzene, toluene, hexane, 2-propanol) or with other Brønsted acids [CH_3SO_3H, CF_3SO_3H, $(CF_3SO_2)_2NH$, picric acid] as well as Lewis acids [$BF_3{\cdot}OEt_2$, $MgBr_2{\cdot}OEt_2$, $AgPF_6$, $ZnCl_2$], but almost no or slight change was observed with ethyl acetate, THF, CH_3CO_2H, $C_6H_5CO_2H$, or phenol (Fig. 4). The dependency of the spectral change on the amount of acid indicated that the reaction is under equilibrium in the acidic conditions (Fig. 3a, S7a). The yellow color of BC and the absorption in the UV-Vis-NIR spectrum were in turn recovered by the addition of NEt_3 to neutralize CF_3CO_2H (Fig. 5a). The recovery yield of BC was determined to be 72% based on the absorption intensity at 461 nm. The ^1H NMR spectrum of BC in freshly distilled CD_2Cl_2 shows slightly broad signals associated with BC and the signals become sharper by addition of 200 mol% NEt_3 to neutralize the trace amount of contaminant acid (Fig. 6). In contrast, the addition of 200 mol% CF_3CO_2H resulted in the disappearance of the signals due to significant broadening, which suggests the generation of a paramagnetic radical species. This result prompted us to measure the ESR spectrum, in which a signal of the radical species from BC with CF_3CO_2H in CH_2Cl_2 was observed (Fig. 7a). These results clearly demonstrate that the acid-responsiveness of BC is not caused by simple protonation/deprotonation or tautomerization,

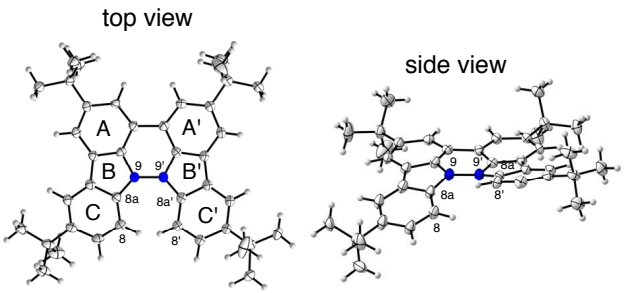

Fig. 2 ORTEP drawings of BC at 50% probability level obtained by X-ray crystallographic analysis. The disorder of a *t*-butyl group is omitted for clarity.

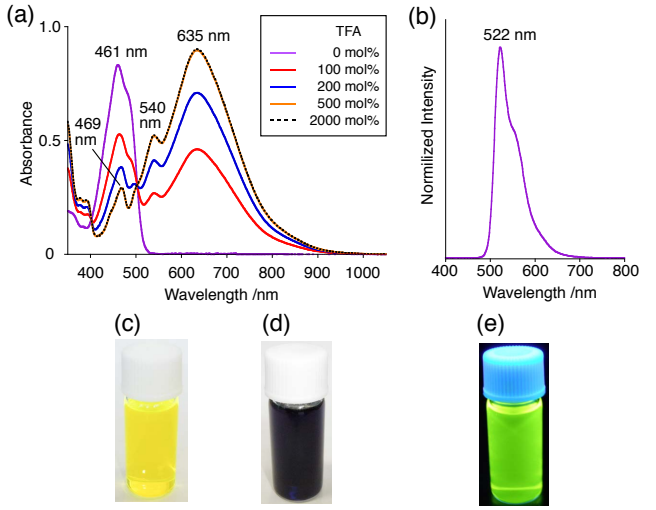

Fig. 3 (a) UV-Vis-NIR spectral change of BC (1.00 mM) by addition of 0, 100, 200, 500, 2000 mol% CF_3CO_2H in CH_2Cl_2 with 1 mm cell. (b) Emission spectrum of BC (0.18 mM) in CH_2Cl_2 (excited at 460 nm). (c) Photo of the solution of BC (1.0 mM) in CH_2Cl_2. (d) Photo of the solution of BC (1.0 mM) with 2000 mol% CF_3CO_2H in CH_2Cl_2. (e) Photo of the solution of BC (1.0 mM) in CH_2Cl_2 under UV light.

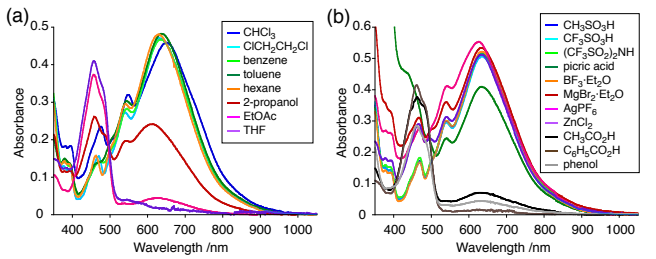

Fig. 4 (a) UV-Vis-NIR spectral change of BC (5.00×10^{-2} mM) by addition of 2000 mol% CF_3CO_2H in organic solvents. (b) UV-Vis-NIR spectral change of BC (5.00×10^{-2} mM) by addition of 2000 mol% acids (10000 mol% picric acid and CH_3CO_2H) in CH_2Cl_2.

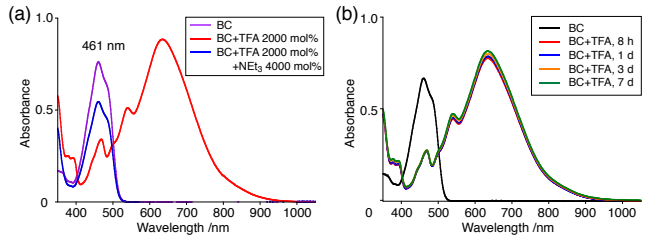

Fig. 5 (a) UV-Vis-NIR spectra of BC (1.00 mM), BC with 2000 mol% CF_3CO_2H, and BC with 2000 mol% CF_3CO_2H followed by 4000 mol% NEt_3 in CH_2Cl_2 with 1 mm cell. (b) UV-Vis-NIR spectra of BC (1.00 mM) with 2000 mol% CF_3CO_2H in CH_2Cl_2 after 8 h, 1 d, 3 d, 7 d in dark at 20 °C under air with 1 mm cell.

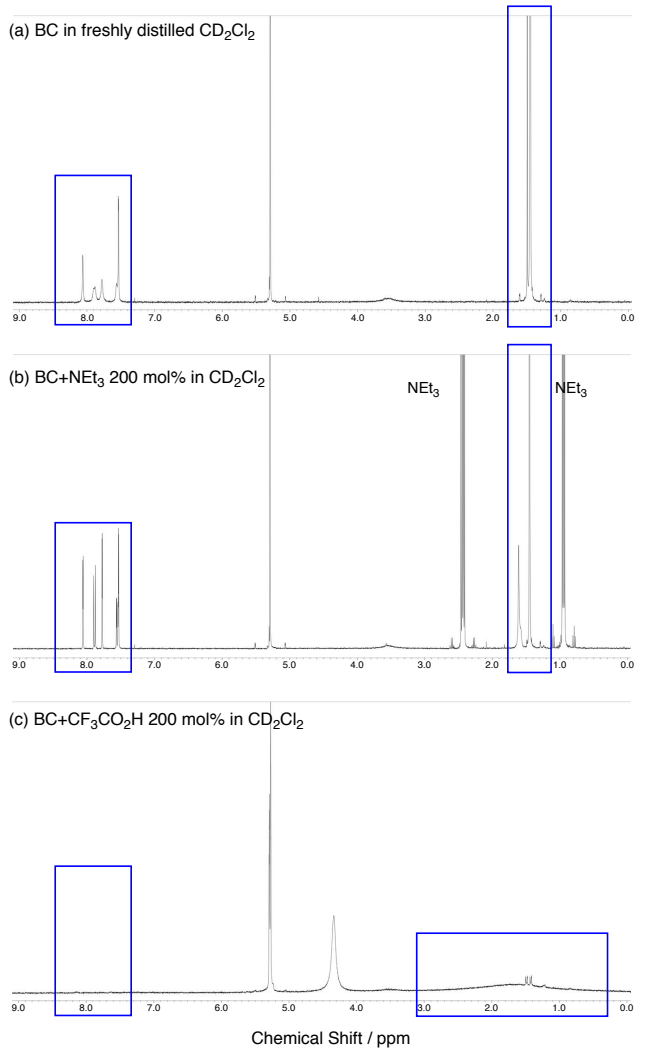

Fig. 6 (a) ^1H NMR spectrum of BC in freshly distilled CD_2Cl_2. (b) ^1H NMR spectrum of BC with 200 mol% NEt_3 in CD_2Cl_2. (c) ^1H NMR spectrum of BC with 200 mol% CF_3CO_2H in CD_2Cl_2.

but is the result of an acid-responsive generation of a radical species involving the homolytic cleavage of a bond or the electron transfer of BC under equilibrium. In addition, the surprising point is the remarkably high stability of the radical species. These experiments can be conducted under air at room temperature without special handling, and no decomposition

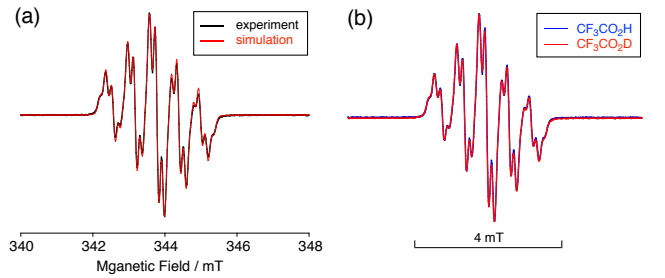

Fig. 7 (a) ESR spectrum of BC (1.02 mM) with 2000 mol% CF_3CO_2H in CH_2Cl_2 at room temperature (X-band, v = 9.637256 GHz, g = 2.0030) and the simulated spectrum (S = 1/2, *hfc a* = 6.0 G with two nitrogens and 1.8, 1.4, 0.2, 0.2, 0.2 G with ten hydrogens, Gaussian linewidth = 0.119 mT, Lorentzian linewidth = 0.019 mT). (b) Comparison of ESR spectra of BC with 2000 mol% CF_3CO_2H and CF_3CO_2D in CH_2Cl_2 at room temperature.

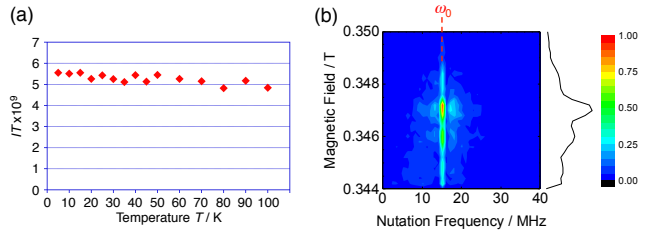

Fig. 8 (a) Temperature dependence of IT value (I=double integral of ESR signal, T=temperature) of BC (1.02 mM) with 2000 mol% CF_3CO_2H in frozen CH_2Cl_2 at 5-100 K. (b) Electron spin transient nutation (ESTN) spectrum of BC (1.0 mM) with 200 mol% CF_3CO_2H in frozen toluene at 5 K.

occurs. Indeed, the UV-Vis-NIR spectra of BC with CF_3CO_2H in CH_2Cl_2 scarcely changed even after 7 days in dark at room temperature under air (Fig. 5b), indicating the extremely high stability of the radical species. BC is also recovered by neutralization with NEt_3 in 72% yield from the generated radical species. To elucidate this phenomenon, we further investigated the details of the generated species and the reaction.

The generated radical species was characterized and assigned as the mono-radical cation $BC^{\bullet+}$ (Scheme 1a) from the following results. The nearly quintet ESR signal (Fig. 7a) indicates the delocalization on the bicarbazole structure with hyperfine splitting by two nitrogen atoms. The ESR signal of BC with CF_3CO_2D is almost identical to that with CF_3CO_2H (Fig. 7b), showing no protonation on the nitrogen owing to no hyperfine splitting derived from the proton. No zero-field splitting on the signal at 5 K in frozen CH_2Cl_2 (Fig. S5a) and no forbidden Δm_s=±2 half-field transition indicate that the spin state is a doublet spin (S=1/2). No temperature dependency of the IT value (I=double integral of ESR signal, T=temperature) at 5~100 K in frozen CH_2Cl_2 agrees with the doublet spin state (Fig. 8a). For further confirmation, the electron spin transient nutation (ESTN) spectrum based on the pulsed-ESR technique was measured at 5 K. (Fig. 8b). In the ESTN spectrum, the signal was observed only at the nutation frequency ω_0=15.2 MHz (S=1/2) but not at $\omega_1=\sqrt{2}\omega_0$=21.5 MHz ($S$=1), confirming the doublet spin. Finally, the structure of the doublet-spin radical was determined to be cation radical $BC^{\bullet+}$ by the fact that the UV-Vis-NIR spectrum agrees with that of $BC^{\bullet+}$ generated by the electrochemical or chemical oxidations of BC (Fig. 9). The cyclic voltammogram (CV) of BC shows the two

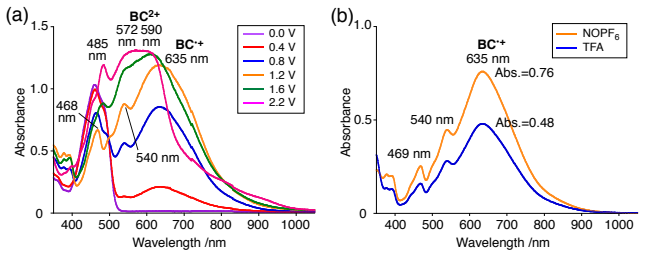

Fig. 9 (a) UV-Vis-NIR spectra of $BC^{\bullet+}$ and BC^{2+} by electrochemical oxidation (vs. Ag/AgCl) with Pt electrode in 1,2-dichloroethane containing 0.1 M Bu_4NClO_4. (b) UV-Vis-NIR spectra of $BC^{\bullet+}$ (5.00×10^{-2} mM) by the chemical oxidation using 150 mol% $NOPF_6$ and that of BC (5.00×10^{-2} mM) with 2000 mol% CF_3CO_2H in CH_2Cl_2.

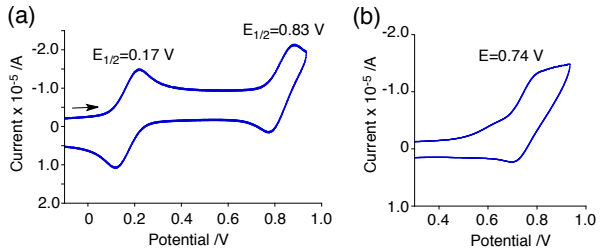

Fig. 10 CV of (a) BC and (b) BCH_2 in CH_2Cl_2 containing 0.1 M Bu_4NClO_4 with a glassy carbon electrode (vs. Fc/Fc^+).

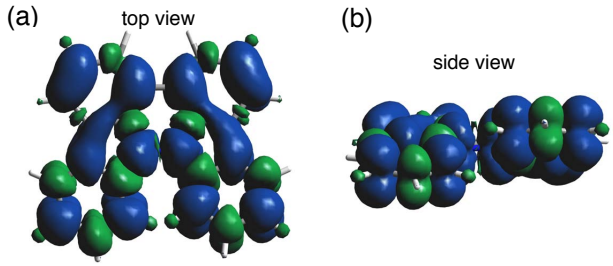

Fig. 11 Calculated spin density distribution of $BC^{\bullet+}$ [UωB97XD/6-31G(d)]. Blue and green colors indicate the positive and negative spin density, respectively.

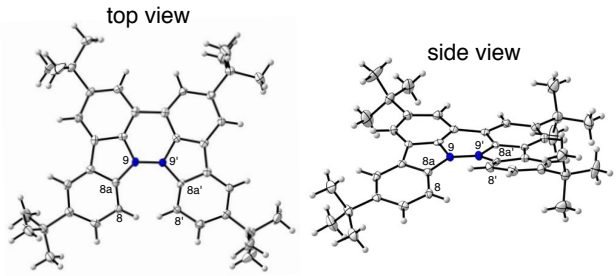

Fig. 12 ORTEP drawings of the cation radical complex $BC^{\bullet+}I_5^-$ at 50% probability level obtained by X-ray crystallographic analysis. Disordered I_5^- and iodobenzene are omitted for clarity.

reversible oxidation waves at 0.17 V and 0.83 V (vs. Fc/Fc^+), where BC is oxidized to $BC^{\bullet+}$ and BC^{2+}, respectively (Fig. 10a). Based on the result of CV, $BC^{\bullet+}$ and BC^{2+} were generated by the electrolysis of BC and the UV-Vis-NIR spectra were measured. UV-Vis-NIR spectrum of electrochemically generated $BC^{\bullet+}$ with the absorption maximum at 635 nm is nearly identical to that of BC with

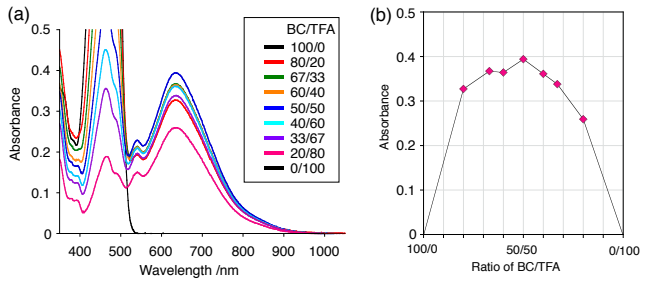

Fig. 13 (a) Continuous variation of UV-Vis-NIR spectra in CH_2Cl_2 by changing the ratio of BC/CF_3CO_2H. The concentration of $BC+CF_3CO_2H$ is 2.00 mM with 1 mm cell. (b) Continuous variation plots of the absorbance at 635 nm versus the ratio of BC/CF_3CO_2H from Fig. 13a.

CF_3CO_2H in 1,2-dichloroethane (Fig. 4a). Chemical oxidations of BC by $NOPF_6$ (Fig. 9b) and I_2 (Fig. S7b) also generate $BC^{\bullet+}$ with the absorption at 635 nm, although the absorption is overlapped with that of I_2 in case of I_2 oxidation. Simulation (EasySpin)[10] of the ESR signal of $BC^{\bullet+}$ afforded the hyperfine coupling (*hfc*) constants a=6.0 G with two nitrogen nuclear spins and 1.8, 1.4, 0.2, 0.2, 0.2 G with ten hydrogens (Fig. 7a). In DFT calculation of $BC^{\bullet+}$ [UωB97XD/6-31G(d)], the spin density is delocalized over the whole bicarbazole skeleton (Fig. 11). The structure of $BC^{\bullet+}$ was confirmed by X-ray crystallographic analysis of the single crystal of the cation radical complex $BC^{\bullet+}I_5^-\cdot IC_6H_5$ obtained from oxidation of BC with I_2 in iodobenzene-MeOH (Fig. 12, S5b, c, S7c). As a characteristic feature of $BC^{\bullet+}$, the N-N bond length (1.35 Å) and the dihedral angle (21 °) of $\angle C_{8a}N_9N_{9'}C_{8a'}$ are shorter and narrower than 1.41 Å and 48 ° of BC, which agrees with the trend ($BC^{\bullet+}$:1.35 Å and 18 °, BC:1.39 Å and 42 °) of DFT calculations.

While $BC^{\bullet+}$ is generated through the one-electron oxidation of BC under acidic conditions, we wondered what the counter oxidant (electron acceptor) was, since there was no added oxidant. The possibility of acid, solvent, or air being the oxidant was discounted because the reaction takes place under several conditions using different kinds of acids or solvents even in anaerobic atmospheres. By combining the experimental and computational data, we finally determined that the reaction is the disproportionation of BC in which BC works as both a one-electron reductant (donor) and a two-electron oxidant (acceptor) (Scheme 1a). In this equation, one equivalent of BC is reduced to BCH_3^+ and two equivalents of BC are oxidized to $BC^{\bullet+}$ with three equivalents of CF_3CO_2H, with the result that three equivalents of BC react with three equivalents of CF_3CO_2H. This reaction formula ($BC:CF_3CO_2H$ = 1:1) was determined by Job's continuous variation plot (Fig. 13).[11] UV-Vis-NIR absorption spectra were measured by changing the ratio of BC to CF_3CO_2H with a constant total concentration of $BC+CF_3CO_2H$ = 2.00 mM (Fig. 13a). The absorbance of $BC^{\bullet+}$ at 635 nm was chosen for the Job's continuous variation plot because only $BC^{\bullet+}$ possesses an absorption at 635 nm, whereas BC, CF_3CO_2H, and BCH_3^+ do not (Fig. 3a, S7e). The plot afforded the maximum value at a ratio of $BC:CF_3CO_2H$ = 50:50 (Fig. 13b), indicating that the constituent of BC and CF_3CO_2H is 1:1. According to the equation in Scheme 1a, 2/3 of BC would be converted to $BC^{\bullet+}$, giving a 67% yield. This yield was determined by comparison of the absorbance intensity of $BC^{\bullet+}$ between the acidic condition (2000 mol% CF_3CO_2H) and the chemical oxidation condition ($NOPF_6$) using the same concentration of BC (Fig. 9b). In the chemical oxidation, the

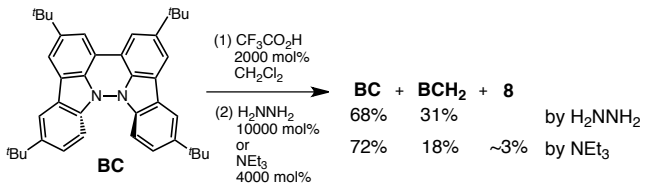

Scheme 4 Quenching experiment of disproportionation of BC

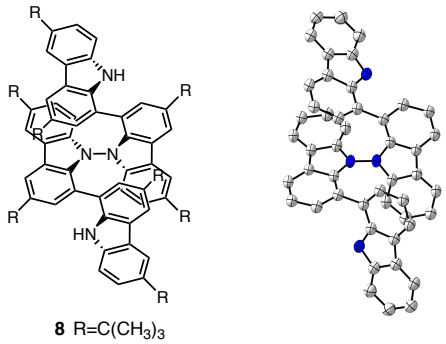

Fig. 14 Structure and ORTEP drawings of 8 at 50% probability level obtained by X-ray crystallographic analysis. Hydrogens and *t*-butyl groups are omitted for clarity.

absorbance of $BC^{\bullet+}$at 635 nm was saturated at 0.76 under the condition that all BC is quantitatively oxidized to $BC^{\bullet+}$ by addition of $NOPF_6$, while the absorbance in the acidic condition was saturated at 0.48. Thus, 0.48/0.76 = 63% of $BC^{\bullet+}$ is generated in the acidic condition. The formation of BCH_3^+ was also indicated by UV-Vis-NIR spectral measurements. From the spectrum of the mixture of $BC^{\bullet+}$ and BCH_3^+ obtained by BC with 2000 mol% CF_3CO_2H was subtracted the spectrum of $BC^{\bullet+}$, giving a nearly identical spectrum to that of BCH_3^+ (Fig. S7d, e, f). The formation of BCH_3^+ was also confirmed by the quenching experiments of the generated $BC^{\bullet+}$ and BCH_3^+ by hydrazine or NEt_3 (Scheme 4, Fig. 5a). After the formation of $BC^{\bullet+}$ and BCH_3^+ from BC with 2000 mol% CF_3CO_2H, quench by 10000 mol% hydrazine afforded BC in 68% isolated yield and BCH_2 in 31% isolated yield. The quench by 4000 mol% NEt_3 also afforded BC in 72% isolated yield and BCH_2 in 18% isolated yield with tetracarbazole **8** (Fig. 14) in ~3% yield as a by-product. These experiments clearly confirmed the disproportionation reaction in Scheme 1a. The equilibrium constant and Gibbs free energy were determined as $K = 1.0\times10^9$ M^{-3} and ΔG = 12 kcal/mol (298 K) in CH_2Cl_2 from the spectrum of BC with 200 mol% CF_3CO_2H (Fig. 3a, absorbance = 0.71 at 635 nm) and $\varepsilon = 1.5\times10^4$ L mol^{-1} cm^{-1} of $BC^{\bullet+}$ at 635 nm (Fig. 9b, $NOPF_6$).

Reversible disproportionation of tetramethyl-4,4',10,10'-biacridine (TBA).

The X-ray crystallographic analysis of TBA also showed a helical molecular shape with the dihedral angle $\angle C_{5a}N_{10}N_{10'}C_{5a'}$ = 83 ° and the C_5-$C_{5'}$ distance 3.61 Å)(Fig. 15), which is wider than those of BC. TBA was also found to undergo the acid-responsive electron transfer disproportionation (Scheme 1b) in the similar manner to BC, which was fully identified by experiments and calculation. While ^{1}H NMR spectrum of TBA in freshly distilled CD_2Cl_2 or with 1000 mol% NEt_3 clearly showed the signals associated with TBA, the ^{1}H NMR spectrum with CF_3CO_2H showed almost no signals due to the generation

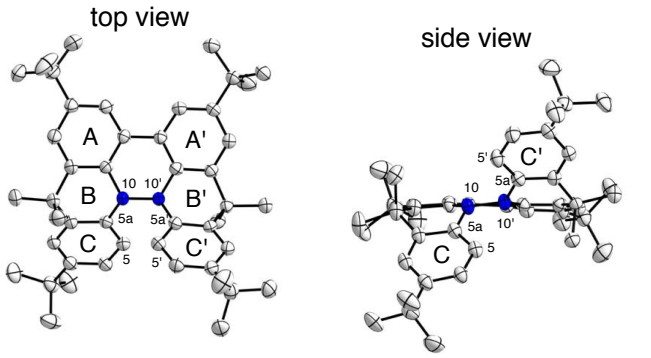

Fig. 15 ORTEP drawings of TBA at 50% probability level obtained by X-ray crystallographic analysis. Hydrogens are omitted for clarity.

of paramagnetic radical species (Fig. S9). The solution of TBA in CH_2Cl_2 showed yellow color and green emission (Fig. 16b, e). The UV-Vis-NIR spectrum of TBA indicated the absorption maximum in visible region is λ_{max} = 412 nm and the emission spectrum indicated the emission maximum is λ_{max} = 518 nm (Fig. 16a, d) with 17% quantum yield in benzene. By treatment of CF_3CO_2H, the color of the solution changed to deep violet under either aerobic or anaerobic conditions (Fig. 16c). In UV-Vis-NIR spectra, the absorption of TBA at λ_{max} = 412 nm was decreased and a new broad absorption at λ_{max} = 824 nm of $TBA^{\bullet+}$ was increased in the visible to near infrared light region (Fig. 16a, S8a) along with the disappearance of fluorescence (Fig. 16d, f). The increase of band at 824 nm was nearly saturated by addition of 400-2000 mol% CF_3CO_2H. Similar changes were also observed in other organic solvents ($CHCl_3$, CCl_4, 1,2-dichloroethane, hexane, benzene, toluene, anisole) or with other weak Brønsted acids (CCl_3CO_2H, picric acid) as well as Lewis acids [$MgBr_2{\cdot}OEt_2$, $ZnCl_2{\cdot}OEt_2$], but almost no or slight change was observed with ethyl acetate, THF, CH_3CO_2H, phenol, $C_6H_5CO_2H$, $LiClO_4$, or LiCl (Fig. S8b, c). The reaction is under equilibrium in the acidic conditions, as indicated by the dependency of the spectral change on the amount of acid and the concentration (Fig. 16a, S8d). In ESR spectral measurements, a signal of $TBA^{\bullet+}$ from TBA with CF_3CO_2H in CH_2Cl_2 was observed (Fig. 16g), while no signal was observed for TBA with NEt_3. The ESR spectrum was fitted using a simulation with *hfc* constants a = 7.1 G with two nitrogen nuclear spins and 1.0, 0.5, 0.3, 0.3, and 0.2 G with ten hydrogens (Fig. 16g), which agrees with the structure of $TBA^{\bullet+}$ with the delocalized unpaired electron over the entire biacridine skeleton (Fig. S12a). The identical ESR spectrum with CF_3CO_2D to that with CF_3CO_2H, the lack of observation of the zero-field splitting and the forbidden $\Delta m_s = \pm2$ half-field transition, and no temperature dependency of the *IT* value at 5–80 K also agreed with the doublet spin state of $TBA^{\bullet+}$ (Fig. S6a, b). The UV-Vis-NIR spectrum of $TBA^{\bullet+}$ generated from TBA with CF_3CO_2H agreed with those of $TBA^{\bullet+}$ formed by the electrochemical or chemical (I_2, DDQ, $NOPF_6$) oxidation of TBA (Fig. 16h, i), confirming that the radical species is $TBA^{\bullet+}$. $TBA^{\bullet+}$ also exhibited high stability in the acidic conditions. The UV-Vis-NIR spectra scarcely changed even after 13 days in dark at room temperature under air (Fig. 16j). The comparison between the absorbance intensity (0.53) of $TBA^{\bullet+}$ under the acidic condition and that (0.78) under the DDQ or I_2 oxidation condition determined 68% (0.53/0.78) formation of $TBA^{\bullet+}$ from the 2/3 part of TBA (Fig. 16i). The formation of $TBAH_4^{2+}$ was indicated by UV-Vis-NIR spectra. Subtraction between the

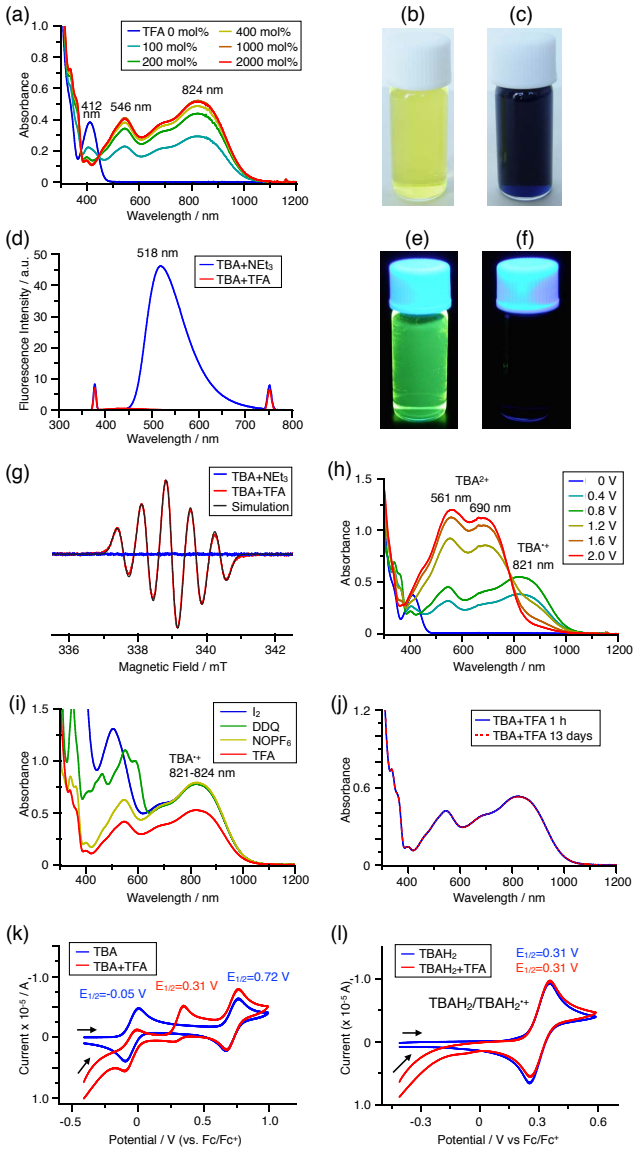

Fig. 16 (a) UV-Vis-NIR spectral change of TBA (0.100 mM) by addition of 0-2000 mol% CF_3CO_2H in CH_2Cl_2. (b) Photo of the solution of TBA (5.00 mM) in CH_2Cl_2. (c) Photo of the solution of TBA (1.00 mM) with 2000 mol% CF_3CO_2H in CH_2Cl_2. (d) Emission spectrum of TBA (0.030 mM) with 500 mol% NEt_3 and TBA with 2000 mol% CF_3CO_2H in CH_2Cl_2 (excited at 378 nm). (e) Photo of the solution of TBA (5.00 mM) in CH_2Cl_2 under UV light. (f) Photo of the solution of TBA (1.00 mM) with 2000 mol% CF_3CO_2H in CH_2Cl_2 under UV light. (g) ESR spectrum of TBA (0.100 mM) with 1000 mol% NEt_3 and TBA with 2000 mol% CF_3CO_2H in CH_2Cl_2 at room temperature (X-band, ν = 9.506032 GHz, g = 2.0036) and the simulated spectrum (S = 1/2, *hfc a* = 7.1 G with two nitrogens and 1.0, 0.5, 0.3, 0.3, 0.2 G with 10 hydrogens). (h) UV-Vis-NIR spectra of $TBA^{\bullet+}$ and TBA^{2+} by electrochemical oxidation (vs. Ag/AgCl) with Pt electrode in 1,2-dichloroethane containing 0.1 M Bu_4NClO_4. (i) UV-Vis-NIR spectra of $TBA^{\bullet+}$ (0.100 mM) by the chemical oxidation using 1000 mol% I_2, 500 mol% DDQ in 1,2-dichloroethane, and 100 mol% $NOPF_6$ in CH_2Cl_2, and the spectrum of TBA (0.100 mM) with 2000 mol% CF_3CO_2H in CH_2Cl_2. (j) UV-Vis-NIR spectra of TBA (0.100 mM) with 2000 mol% CF_3CO_2H in CH_2Cl_2 after 1 h and 13 d in dark at 20 °C under air. (k) CV of TBA and TBA with 2000 mol% CF_3CO_2H and (l) CV of $TBAH_2$ and $TBAH_2$ with 2000 mol% CF_3CO_2H in CH_2Cl_2 containing 0.1 M Bu_4NClO_4 with a Pt electrode (vs. Fc/Fc^+).

spectrum of the mixture of $TBA^{\bullet+}$ and $TBAH_4^{+}$ and that of $TBA^{\bullet+}$gave a nearly identical spectrum to that of $TBAH_4^{+}$ (Fig.

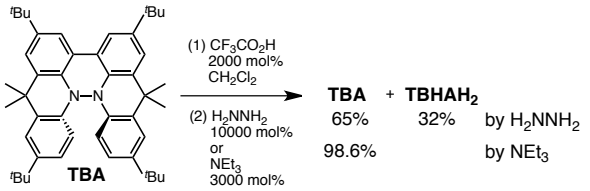

Scheme 5 Quenching experiment of disproportionation of TBA

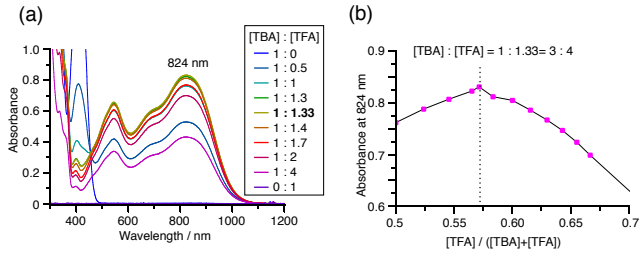

Fig. 17 (a) Continuous variation of UV-Vis-NIR spectra in CH_2Cl_2 by changing the ratio of TBA/CF_3CO_2H. The concentration of TBA+CF_3CO_2H is 4.00 mM with 1 mm cell. (b) Continuous variation plots of the absorbance at 824 nm versus the ratio of TBA/CF_3CO_2H from Fig. 17(a).

S8e, f, g). The existence of $TBAH_4^{2+}$ was also observed by electrochemical analysis (CV)(Fig. 16k, l). While only the oxidations of TBA to $TBA^{\bullet+}$ at $E_{1/2}$ = -0.05 V and further to TBA^{2+} at 0.72 V (vs. Fc/Fc^+) were observed as two reversible waves in the neutral condition, a new oxidation wave at $E_{1/2}$ = 0.31 V appeared in the acidic condition of TBA with CF_3CO_2H, which is consistent with the oxidation potential of $TBAH_2$ at $E_{1/2}$ = 0.31 V. The formation of $TBAH_4^{2+}$ was finally confirmed by the quenching experiment of the generated $TBA^{\bullet+}$ and $TBAH_4^{2+}$ from TBA with CF_3CO_2H by hydrazine, giving TBA in 65% isolated yield and $TBAH_2$ in 32% isolated yield (Scheme 5).

While the reaction of TBA is similar to that of BC, three informative differences were admitted. One difference is the reaction formula of TBA and CF_3CO_2H (Scheme 1). Job's continuous variation plot (Fig. 17, S8h) determined the ratio of TBA:CF_3CO_2H as 3:4, while that of BC:CF_3CO_2H is 3:3 (Fig. 13). Thus, the reduced product $TBAH_2$ is concluded to be di-protonated, whereas BCH_2 is mono-protonated (Scheme 1). This difference is attributed to the more basicity of dimethylacridine than carbazole. The equilibrium constant and Gibbs free energy were determined as $K = 6.5\times10^{17}$ M^{-4} and ΔG = 24 kcal/mol (298 K) in CH_2Cl_2 from the spectrum of TBA with 100 mol% CF_3CO_2H (Fig. 16a, absorbance=0.29 at 824 nm) and $\varepsilon=7.9\times10^3$ L mol^{-1} cm^{-1} of $TBA^{\bullet+}$ at 824 nm (Fig. 16i, $NOPF_6$). Second difference is the remarkable reversibility of the reaction of TBA by neutralization with NEt_3. Upon quenching by 4000 mol% NEt_3 after the conversion of BC to $BC^{\bullet+}CF_3CO_2^-$ and $BCH_3^+2CF_3CO_2^-$ by 2000 mol% CF_3CO_2H in CH_2Cl_2, BC was recovered in 72% yield concomitant with BCH_2 in 18% yield (Fig. 5a, Scheme 4). In contrast, addition of NEt_3 in case of TBA recovered TBA in 98.6% yield based on the absorption intensity at 412 nm (Scheme 5, Fig. 18a, Table S2). The ^1H NMR experiments also demonstrated the high recovery of TBA (Fig. S9). This remarkable high reversibility was further confirmed up to 5th cycle with UV-Vis-NIR spectral measurements by repeating acidification/neutralization with the addition of CF_3CO_2H (~94000 mol%) and NEt_3 (~120000 mol%) to TBA, giving 97.6% recovery yield per cycle in average based on the

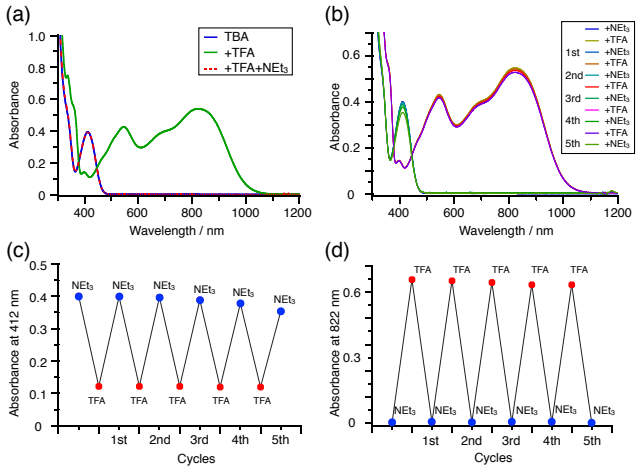

Fig. 18 (a) UV-Vis-NIR spectra of TBA (0.100 mM), TBA with 2000 mol% CF_3CO_2H, and TBA with 2000 mol% CF_3CO_2H followed by 3000 mol% NEt_3 in CH_2Cl_2. (b) UV-Vis-NIR spectra by repeating acidification/neutralization with the addition of CF_3CO_2H and NEt_3 to TBA (0.100 mM) in CH_2Cl_2 up to 5th cycles. (c) Absorbance at 412 nm and (d) that at 822 nm in UV-Vis-NIR spectra [Fig. 18(b)] by repeating acidification/neutralization with the addition of CF_3CO_2H and NEt_3 to TBA in CH_2Cl_2 up to 5th cycles.

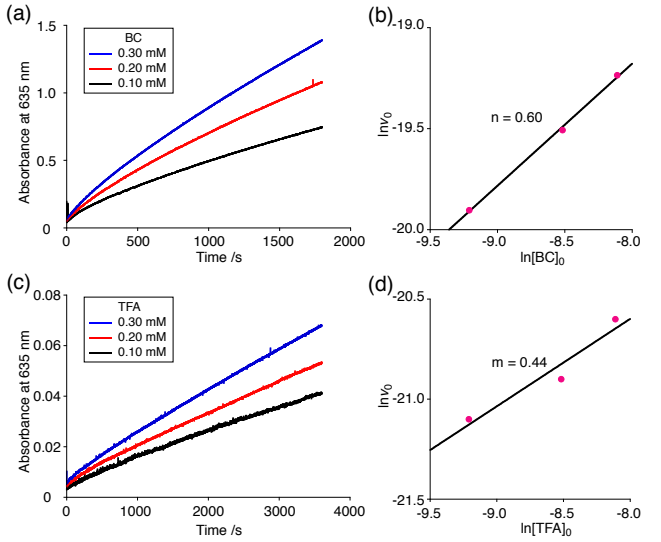

Fig. 19 (a) Time-dependent change of the absorbance of $BC^{\bullet+}$ at 635 nm by mixing BC (0.10, 0.20, 0.30 mM) and TFA (5.00 mM) in CH_2Cl_2 at 20 °C. (b) The reaction order in BC from the plot of $\ln[BC]_0$ versus $\ln v_0$ using the data in Fig. 19(a). (c) Time-dependent change of the absorbance of $BC^{\bullet+}$ at 635 nm by mixing BC (5.00 mM) and TFA (0.10, 0.20, 0.30 mM) in CH_2Cl_2 at 20 °C. (d) The reaction order in TFA from the plot of $\ln[TFA]_0$ versus $\ln v_0$ using the data in Fig. 19(c).

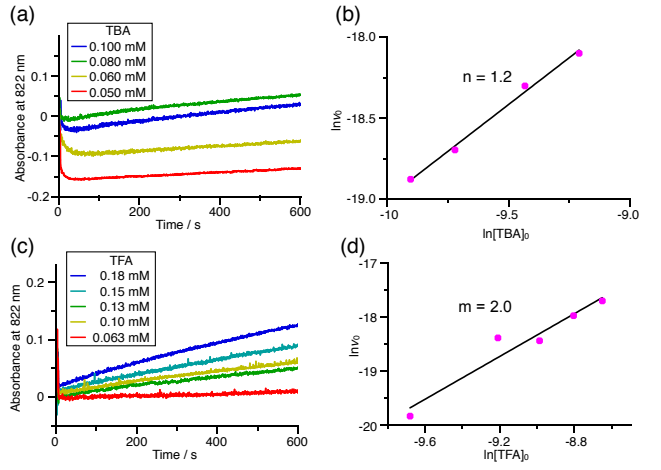

Fig. 20 (a) Time-dependent change of the absorbance of $TBA^{\bullet+}$ at 822 nm by mixing TBA (0.100, 0.080, 0.060, 0.050 mM) and TFA (2.00 mM) in CH_2Cl_2 at -70 °C. (b) The reaction order in TBA from the plot of $\ln[TBA]_0$ versus $\ln v_0$ using the data in Fig. 20(a). (c) Time-dependent change of the absorbance of $TBA^{\bullet+}$ at 822 nm by mixing TBA (5.00 mM) and TFA (0.18, 0.15, 0.13, 0.10, 0.063 mM) in CH_2Cl_2 at -60 °C. (d) The reaction order in TFA from the plot of $\ln[TFA]_0$ versus $\ln v_0$ using the data in Fig. 20(c).

absorbance at 412 nm (Fig. 18b, c, d). The difference of this remarkable high reversibility was attributed to the difference of redox potentials between BC and TBA. Third difference is the reaction mechanism regarding to the reaction order at N-N bond cleavage step. The differences of the reversibility of reaction and the reaction order are discussed in the following mechanism chapters.

Reaction mechanism of disproportionation

The proposed mechanisms of electron transfer disproportionation reactions of BC and TBA are shown in Scheme 6 and 7,[12] featuring the acid-triggered N-N bond cleavage reactions to generate electrophilic open-shell singlet biradical species followed by the electron transfer. Upon acidification, BC or TBA undergoes protonation by CF_3CO_2H, followed by thermal retro-6π-electrocyclization[13] to cleave N-N bond, giving the open-shell singlet biradical intermediate $BCH^{\bullet\bullet+}$ or $TBAH_2^{\bullet\bullet2+}$. Electron transfer from electron-rich BC or TBA to electron-deficient $BCH^{\bullet\bullet+}$ or $TBAH_2^{\bullet\bullet2+}$ and protonation afford one equivalent of BCH_3^+ or $TBAH_4^{2+}$ and two equivalents of $BC^{\bullet+}$ or $TBA^{\bullet+}$, respectively. The different reaction mechanisms at N-N bond cleavage steps, i.e. mono-protonation mechanism of BC and di-protonation mechanism of TBA, are proposed based on the results of kinetic experiments. Kinetic studies of the reaction of BC with CF_3CO_2H at different concentrations by the method of initial rates (Fig. 19, S10, Table S4, 5) determined that the reaction orders in BC and CF_3CO_2H are 0.6 and 0.4 in both CH_2Cl_2 and benzene, respectively. This reaction order can be explained by the reaction model in Scheme 8; (1) BC and CF_3CO_2H has equilibrium with BCH^+ and $CF_3CO_2^-$ with an equilibrium constant $K_1 = [BCH^+][CF_3CO_2^-]/[BC][CF_3CO_2H]$, (2) the intermediate BCH^+ undergoes N-N bond cleavage reaction. With this model, the reaction rate v is 1st order in BCH^+.

$$v = k_1[BCH^+]$$

Under the condition of $[BCH^+] = [CF_3CO_2^-]$, $[BCH^+]$ is given as

$$[BCH^+] = K_1^{1/2}[BC]^{1/2}\,[CF_3CO_2H]^{1/2}$$

Thus, the reaction rate is 0.5 order in each BC and CF_3CO_2H, which are consistent to the observed reaction orders.

$$v = k_1\,K_1^{1/2}[BC]^{1/2}\,[CF_3CO_2H]^{1/2}$$

With the reaction model, the activation barrier energy of BC in CH_2Cl_2 was determined to be $\Delta G^{\ddagger} = 28$ kcal/mol (293 K)(Table

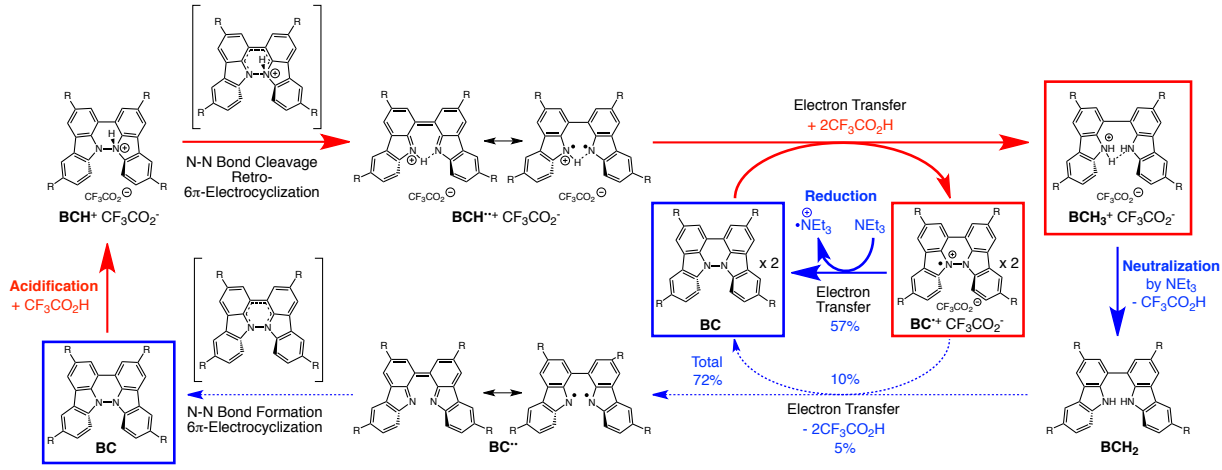

Scheme 6 Proposed reaction mechanism of disproportionation of BC[12]

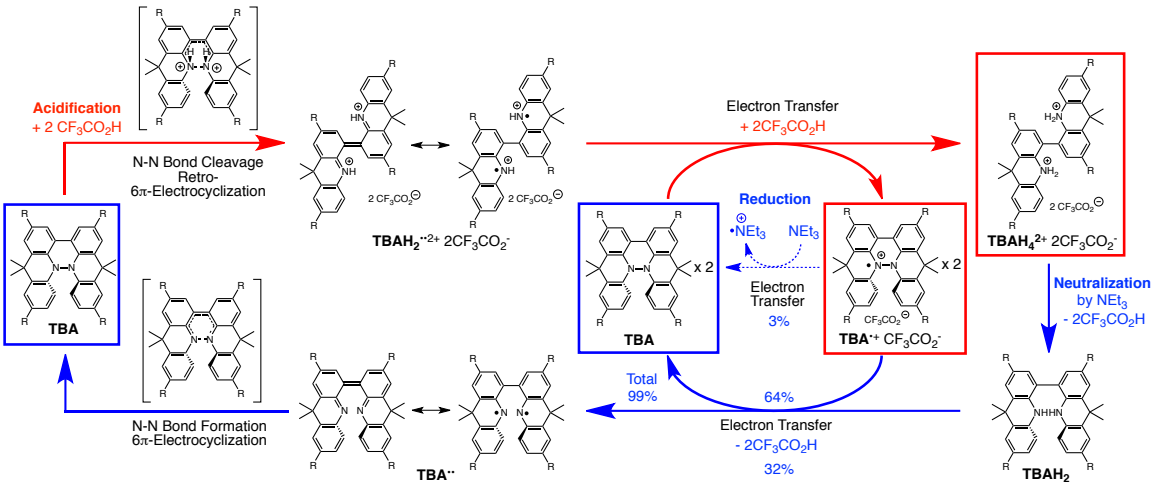

Scheme 7 Proposed reaction mechanism of disproportionation of TBA[12]

S4, 5). On the other hand, the kinetic experiments of TBA showed that the reaction is 1st order in TBA and 2nd order in CF_3CO_2H (Fig. 20, Table S6, 7), indicating that the di-protonation to TBA undergoes the N-N bond cleavage reaction [Scheme 8(3)]. The N-N bond cleavage reaction of TBA through di-protonation rather than mono-protonation is consistent to the more basicity of TBA than that of BC. The activation barrier energy of TBA in CH_2Cl_2 was determined to be $\Delta G^{\ddagger} = 11$ kcal/mol (293 K)(Fig. S11, Table S8). The value is very lower than 28 kcal/mol of BC, showing that the reaction of TBA with CF_3CO_2H is much faster than that of BC. In case of BC, di-protonation pathway would be disfavored than mono-protonation due to the less basicity. These results of kinetic experiments also validate that the reactions go though the N-N bond cleavage from BCH^+ to $BCH^{\bullet+}$ or from $TBAH_2^{2+}$ to $TBAH_2^{\bullet 2+}$ as the rate-determining step before the electron transfer, but not the bimolecular electron transfer reaction from BC to BCH^+ or from TBA to $TBAH_2^{2+}$ as the rate-determining step, because the reaction would be 2nd order in BC or TBA in the latter implausible mechanism.

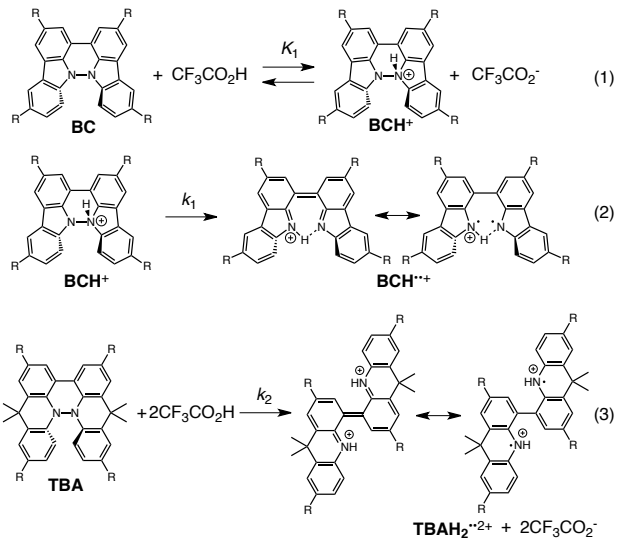

Scheme 8 Proposed Reaction Mechanism of N-N bond cleavage step of BC and TBA[12]

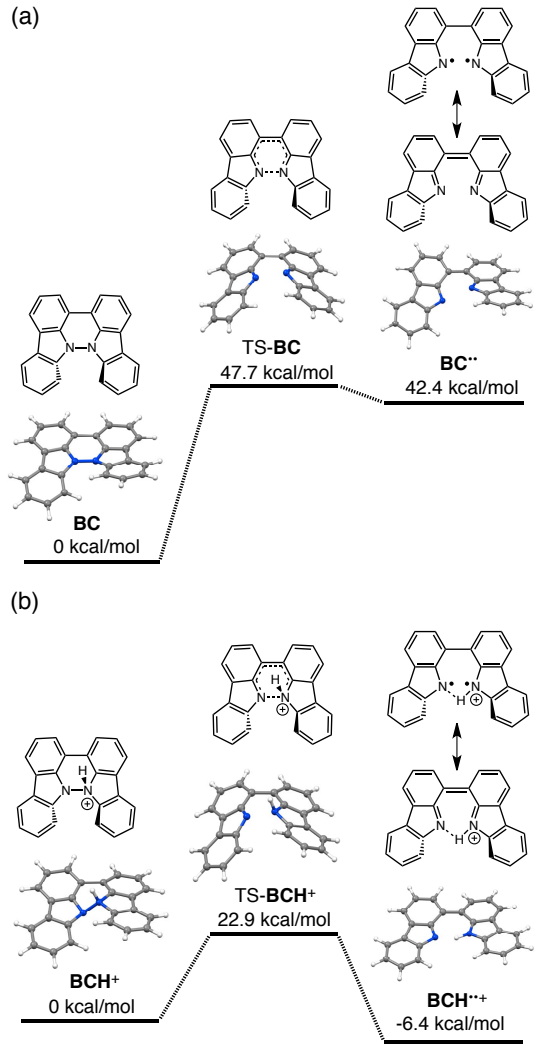

Fig. 21 DFT calculations of the N-N bond cleavage/formation reactions of BC [UωB97XD/6-31G(d)]. (a) Neutral condition. (b) Mono-protonated condition. *t*-Butyl groups are omitted for calculation.

The reaction mode of the N-N bond cleavage reactions must be thermally allowed disrotatory retro-6π-electrocyclization.[13] The N-N bond cleavage reaction processes under neutral and acidic conditions were further examined by density functional theory (DFT) calculations [UωB97XD/6-31G(d)] for the validation (Fig. 21, 22).[12] In the neutral condition (Fig. 21a, 22a), the activation energy for the disrotatory retro-6π-electrocyclization is very high (TS-BC: 47.7 kcal/mol, TS-TBA: 47.8 kcal/mol), and BC and TBA are thermodynamically much more stable than the open-shell singlet biradical states[14] (BC$^{\bullet\bullet}$: 42.4 kcal/mol, TBA$^{\bullet\bullet}$: 23.8 kcal/mol) after the N-N bond cleavage. Thus, the N-N bond cleavage reactions do not to take place under neutral conditions. In contrast, by mono-protonation to BC under the acidic condition (Fig. 21b), the calculated barrier energy from the mono-protonated BCH$^+$ to the transition state TS-BCH$^+$ becomes lower (+22.9 kcal/mol) and the open-shell singlet state[14] BCH$^{\bullet\bullet+}$ comes to more stable (-6.4 kcal/mol) than BCH$^+$. This calculated barrier energy is consistent to the experimental value ($\Delta G^{\ddagger}$ = 28 kcal/mol) by accounting the protonation energy from BC to BCH$^+$, which demonstrates the high validity of the N-N bond cleavage

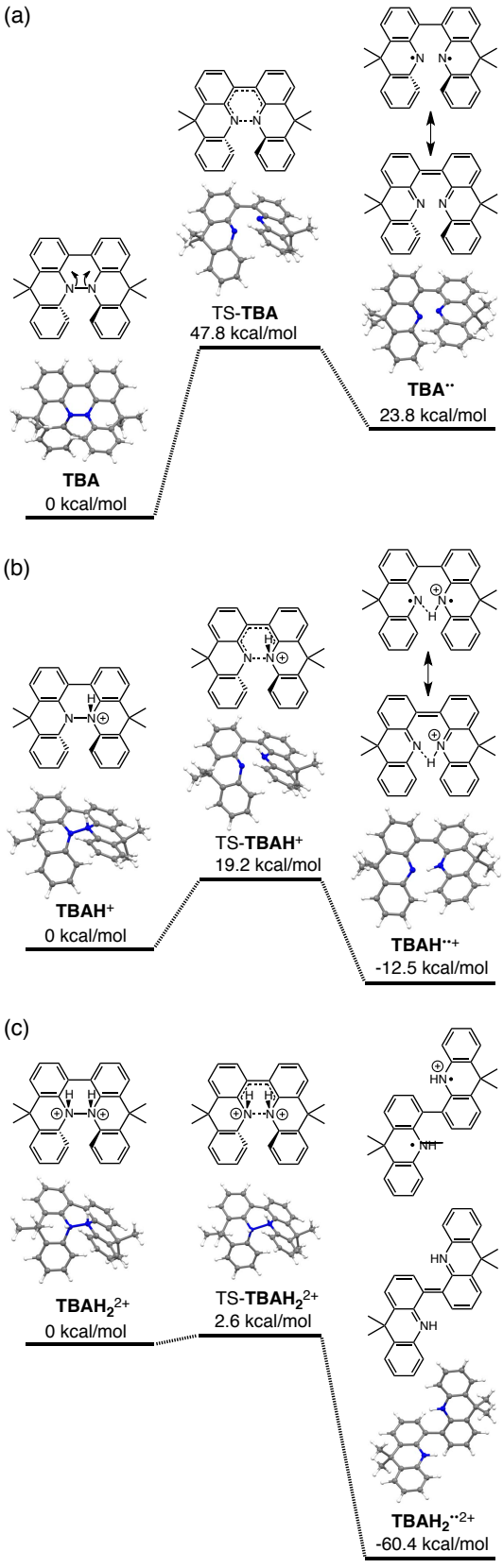

Fig. 22 DFT calculations of the N-N bond cleavage/formation reactions of TBA [UωB97XD/6-31G(d)]. (a) Neutral condition. (b) Mono-protonated condition. (c) Di-protonated condition. *t*-Butyl groups are omitted for calculation.

reaction under the acidic condition. The value of barrier energy from BCH^+ to TS-BCH^+ also supports the proposed reaction model that BCH^+ exists as the intermediate [Scheme 6, 8(1)(2)]. Both mono-protonation and di-protonation mechanisms were calculated for the acidic condition of TBA (Fig. 22 b, c). In case of di-protonation, *cis*-di-protonation to TBA is necessary for the thermal disrotatory retro-6π-electrocyclization. In both cases, the calculated barrier energies from mono-protonated $TBAH^+$ to TS-$TBAH^+$ and from *cis*-di-protonated $TBAH_2^{2+}$ to TS-$TBAH_2^{2+}$ also become lower (TS-$TBAH^+$: +19.2 kcal/mol, TS-$TBAH_2^{2+}$: +2.6 kcal/mol) and the open-shell singlet states[14] are more stable ($TBAH^{\bullet\bullet+}$: -12.5 kcal/mol, $TBAH_2^{\bullet\bullet+}$: -60.4 kcal/mol), supporting the N-N bond cleavage reaction under the acidic conditions. By accounting the protonation energy, the di-protonation mechanism is consistent to the experimental barrier energy ($\Delta G^{\ddagger}$ = 11 kcal/mol). Although the barrier energy of the mono-protonation mechanism is also acceptable for the reaction of TBA to proceed, the calculated values indicate that the di-protonation mechanism is faster than the mono-protonation mechanism. The experimental reaction orders and the relatively small calculated barrier (+2.6 kcal/mol) between $TBAH_2^{2+}$ and TS-$TBAH_2^{2+}$ suggest that $TBAH_2^{2+}$ is not the intermediate and the *cis*-di-protonation to TBA undergoes the N-N bond cleavage reaction without an intermediate [Scheme 7, 8 (3)]. After the formation of electron-deficient $BCH^{\bullet\bullet+}$ or $TBAH_2^{\bullet\bullet2+}$, electron transfer from electron-rich BC or TBA takes place (Scheme 7, 8). The results of electrochemical analysis (Fig. 10a, b, 16 k, l, Table 1) indicate that the lower oxidation potentials of BC (0.17 V) or TBA (-0.05 V) than those of BCH (0.74 V) or $TBAH_2$ (0.31 V) promote the electron transfer from BC to $BCH^{\bullet\bullet+}$ or from TBA to $TBAH_2^{\bullet\bullet2+}$. The protonation to BCH_3^+ or $TBAH_4^{2+}$ also assists the electron transfer process under equilibrium under acidic conditions (Scheme 6, 7). No observation of NMR signals of BC and BCH_3^+ or TBA and $TBAH_4^{2+}$ even in the presence of small amount of acids indicates that the electron transfer is under fast equilibrium.

Table 1 Electrochemical oxidation potentials[a]

BC	BCH	TBA	$TBAH_2$	NEt_3
0.17 V	0.74 V[b]	-0.05 V	0.31 V	0.45 V[b]

[a] In CH_2Cl_2 containing 0.1 M Bu_4NClO_4 (vs. Fc/Fc^+). [b] Differential pulse voltammetry (DPV).

Reaction mechanism of the reversible disproportionation

The proposed mechanisms of the recovery of BC or TBA by treatment of NEt_3 from the disproportionation are shown in Scheme 6 and 7. The reversible reaction of TBA features the back electron transfer and the N-N bond formation enabled by the acid-regulated N-N bond cleavage/formation reactions as an efficient switching mechanism and the balance of the redox potentials. The difference on the reversibility of reaction between BC and TBA can be explained by the difference of redox potentials versus that of NEt_3 (Table 1). Theoretically, 67% BC^+ and 33% BCH_3^+ or 67% TBA^+ and 33% $TBAH_4^{2+}$ are formed by acidification of BC or TBA through disproportionation. When the mixture was quenched by hydrazine, BCH_3^+ or TBA^+ was reduced by the electron transfer from hydrazine and BCH_3^+ or $TBAH_4^{2+}$ were neutralized by hydrazine nearly simultaneously. Thus, the recovered products (68% BC and 31% BCH_2, or 65% TBA and 32% $TBAH_2$)

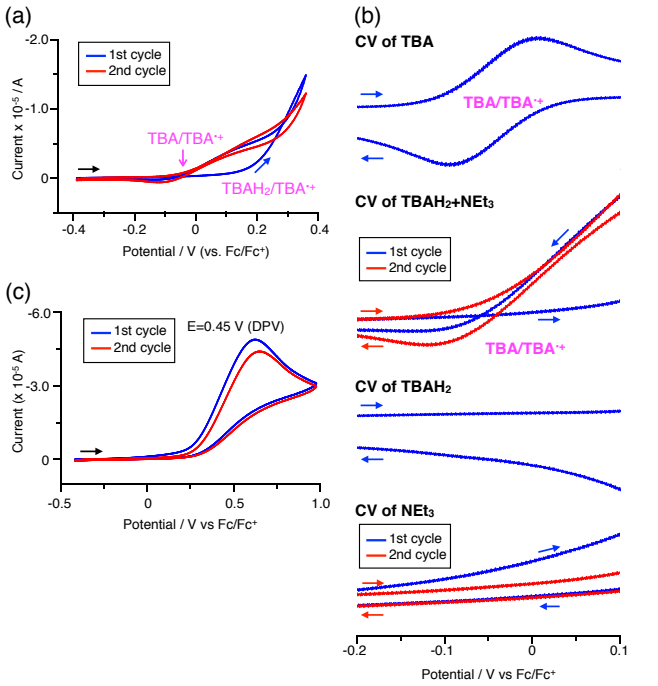

Fig. 23 (a) CV of $TBAH_2$ with 1000 mol% NEt_3 in CH_2Cl_2 containing 0.1 M Bu_4NClO_4 (vs. Fc/Fc^+). (b) Expanded views of CV of TBA (Fig. 16k), $TBAH_2$+NEt_3 (Fig. 23a), $TBAH_2$ (Fig. 16l), and NEt_3 (Fig. 23c)(vs. Fc/Fc^+). (c) CV of NEt_3 in C_2Cl_2 containing 0.1M Bu_4NClO_4 (vs. Fc/Fc^+).

reflected the ratio of the disproportionation products as they were in the reaction (Scheme 4, 5). On the other hand, when the mixture from TBA was quenched by NEt_3, 99% yield of TBA was recovered (Fig. 18a, Scheme 5). This result indicates that NEt_3 works only as a base to neutralize $TBAH_4^{2+}$ to $TBAH_2$, and $TBAH_2$ is converted back to TBA through the back electron transfer between $TBA^{\bullet+}$, the deprotonations by NEt_3, and the N-N bond forming 6π-electrocyclization (Scheme 7). The formation of TBA from $TBAH_2$ was reproduced by the electrochemical oxidation in the presence of NEt_3. Whereas the electrochemical oxidation (CV) of $TBAH_2$ in the absence of NEt_3 showed only a reversible oxidation wave of $TBAH_2/TBAH_2^{\bullet+}$ by sweeping up to 0.59 V (Fig. 16l), the oxidation in the presence of NEt_3 up to 0.36 V converted $TBAH_2$ to $TBA^{\bullet+}$ through the electrochemical oxidations and the deprotonations by NEt_3 from $TBAH_2$ to $TBA^{\bullet\bullet}$, the thermal disrotatory 6π-electrocyclization from $TBA^{\bullet\bullet}$ to TBA, and the electrochemical oxidation from TBA to $TBA^{\bullet+}$, as indicated by the observation of the $TBA^{\bullet+}$/TBA redox wave (Fig. 23a, b). The oxidation potential 0.31 V of $TBAH_2$ is lower than 0.45 V of NEt_3 (Table 1, Fig. 16 l, 23c), which indicates that $TBAH_2$ is a stronger electron donor than NEt_3 to reduce TBA to $TBA^{\bullet+}$. By calculation with the total recovery yield (99%) of TBA, 64% of $TBA^{\bullet+}$ among theoretically formed 67% $TBA^{\bullet+}$ would be reduced by 32% $TBAH_2$ among 33% $TBAH_2$, while 3% of $TBA^{\bullet+}$ would be reduced by NEt_3 (Scheme 7). Judging from the oxidation potentials of TBA (-0.05 V) and $TBAH_2$ (0.31 V), the back electron transfer process between $TBA^{\bullet+}$ and $TBAH_2$ is unfavored. Nevertheless, these redox potentials would be

close enough for the back electron transfer to proceed under equilibrium to form TBA$^{\bullet\bullet}$ with the help of deprotonations by NEt_3. To complete this unfavored equilibrium, the N-N bond forming 6π-electrocyclization plays an important role. Based on the DFT calculation (Scheme 22a), the N-N bond formation reaction from TBA$^{\bullet\bullet}$ to TBA through TS-TBA under neutral condition is much favored to proceed irreversibly, judging from the low activation energy (24.0 kcal/mol from TBA$^{\bullet\bullet}$ to TS-TBA) and the thermodynamic stability of TBA (-23.8 kcal/mol vs. TBA$^{\bullet\bullet}$). Thus, the irreversible formation of stable TBA from TBA$^{\bullet\bullet}$ through the N-N bond formation reaction would shift the equilibrium and complete the backward reaction (Scheme 7). In contrast, when the disproportionation mixture from BC was quenched by NEt_3, only slightly higher yield (72%) of BC and lower yield (18%) of BCH_2 were recovered than those by hydrazine (Fig. 5a, Scheme 4). Based on the recovery yield of BC (72%), only 10% of BC$^{\bullet+}$ among theoretically formed 67% BC$^{\bullet+}$ would be reduced by only 5% BCH_2 among 33% BCH_2, while most (57%) of TBA$^{\bullet+}$ would be reduced by NEt_3 (Scheme 6). The oxidation potential 0.74 V of BCH_2 is far from 0.17 V of BC and higher than 0.45 V of NEt_3. Thus, NEt_3 works as a main stronger electron donor to reduce BC$^{\bullet+}$ and only part of BCH_2 reduce BC$^{\bullet+}$ (Scheme 6). These mechanisms indicate that the disproportionation of TBA is really reversible but that of BC is not by neutralization, although moderate yield (72%) of BC is recovered. The recovery of BC is mostly attributed to another reaction to reproduce BC, i.e. reduction by NEt_3.

Related N-N linked polyheterocyclic compounds

Tetraphenylhydrazine **9** (Fig. 24) was reported to undergo acid-promoted homolytic N-N bond cleavage under strong acidic conditions (HCl, H_2SO_4) from early 1900's.[15] However, the generated aminium radical is unstable to give decomposition products in this case. While syntheses and some properties of 9,10-dihydro-9,10-diphenylphenanthroline **10**[16] and biphenothiazine **11a**[17] (Fig. 24) were reported, the reactivity toward acids were not investigated. Judging from the similarity of structures to BC and TBA, compounds **11** to share "a hydrazinohelicene structure" with BC and TBA (Fig. 24) would be the promising substrates to undergo acid-triggered electron transfer disproportionation. Nevertheless, "a diarylphenanthroline structure" of compound **10** in addition to BC, TBA, and **11** could be the required minimum structure for the reaction as well. In order to reveal the scope and limitation of the acid/base-regulated electron transfer disproportionation, the reactivity of related N-N linked polyheterocyclic compounds should be investigated, which is now in progress.

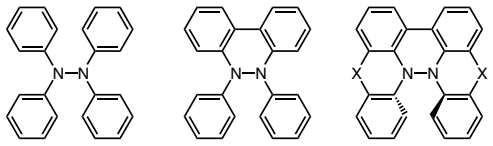

9 **10** **11a** X=S **11b** X=O **11c** X=NR

Fig. 24 Tetraphenylhydrazine 9, 9,10-dihydro-9,10-diphenylphenanthroline 10, biphenothiazine **11a**, biphenoxazine **11b**, and biphenazine **11c**.

Conclusions

After the elucidation of the overall reactions of BC and TBA including the detailed mechanism, it was recognized that the characteristic chemical and physical properties of the components involved in this reaction and the external acid/base stimuli are flawlessly associated with each other to establish this electron transfer reaction. Specifically, the acid-regulated N-N bond cleavage/formation reactions of TBA as an efficient switch even with weak acids and the balanced redox potentials of components establish the highly reversible electron transfer reaction. Importantly, this discovery is not limited to only a finding of an electron transfer disproportionation of two organic molecules, but it also provides new design concepts for acid/base-regulated organic electron transfer systems, reducing/oxidizing chemical reagents, or organic functional materials. The notable chemical and physical properties of BC and TBA such as the excellent multi-electron redox properties and the acid-induced radical formation hold promise for its wide applications.

Acknowledgements

This work was supported by the Japan Society for the Promotion of Science (JSPS) KAKENHI Grant Numbers 25410124 (S. H.), 26102002 (S. H.), 26860005 (K. Y.), 25288013 (Y. K., T. Y.), 25410030 (Y. K.), 26104538 (Y. K.), and 25410158 (K. N.), the Sumitomo Chemical Foundation (S. H.), and the Morino Foundation for Molecular Science (Y. K.). Part of the theoretical calculations was conducted using the resources of Research Center for Computational Science, Okazaki, Japan. We thank H. Sakurai for supporting this project and M. Fujiwara for ESR measurements.

Notes and references

[a] *Institute for Molecular Science, Myodaiji, Okazaki 444-8787, Japan. E-mail: higashi@ims.ac.jp*

[b] *School of Physical Sciences, The Graduate University for Advanced Studies, Myodaiji, Okazaki 444-8787, Japan.*

[c] *Japan Science and Technology Agency, PRESTO, 4-1-8 Honcho, Kawaguchi, Saitama 332-0012, Japan.*

[d] *Center for Instrumental Analysis, Institute for Research Promotion, Niigata University, Nishi-ku, Niigata 950-2181, Japan.*

[e] *Division of Advanced Materials Science, Pohang University of Science and Technology, San 31, Hyojadong, Pohang 790-784, Korea.*

[f] *Japan Science and Technology Agency, ACT-C, 4-1-8 Honcho, Kawaguchi, Saitama 332-0012, Japan.*

† Electronic Supplementary Information (ESI) available: Experimental information, synthesis and characterization data, NMR spectra, solid NMR data, X-ray data, ESR spectra, UV-Vis-NIR spectra, fluorescence spectra, kinetic experiments, theoretical calculation, Table S1-S8, Scheme S1, Figures S1-12, References. See DOI: 10.1039/b000000x/

‡ These authors have contributed equally.

1 (*a*) F. Cicoira, and C. Santato, *Organic Electronics: Emerging Concepts and Technologies*, Wiley-VCH, Weinheim, 2013; (*b*) S. S. Isied, *Electron Transfer Reactions: Inorganic, Organometallic, and Biological Applications*, American Chemical Society, Washington, 1997; (*c*) V. Balzani, *Electron Transfer in Chemistry, Principles, Theories, Methods, and Techniques*, Wiley-VCH, Weinheim, 2001; (*d*) V. K. Ahluwalia, *Oxidations in Organic Synthesis*, CRC Press,

Boca Rayton, 2012; (*e*) V. K. Ahluwalia, *Reduction in Organic Synthesis*, CRC Press, Boca Rayton, 2012; (*f*) R. E. Blankenship, *Molecular Mechanism of Photosynthesis*, Wiley-Blackwell, Oxford, 2014; (*g*) D. Gamenara, G. Seoane, P. S. Méndez and P. D. de María, *Redox Biocatalysis: Fundamentals and Applications*, Wiley, Hoboken, 2012; (*h*) R. K. Murray, D. A. Bender, K. M. Botham, P. J. Kennelly, V. W. Rodwell and P. A. Weil, *Harpers Illustrated Biochemistry 29th Edition*, McGraw-Hill, 2012.

2 (*a*) S. Torii, *Electroorganic Reduction Synthesis*, Wiley-VCH, Weinheim, 2006; (*b*) Y. Tachibana, L. Vayssieres and J. R. Durrant, *Nat. Photonics* 2012, **6**, 511; (*c*) C. K. Prier, D. A. Rankic and D. W. C. MacMillan, *Chem. Rev.* 2013, **113**, 5322.

3 M. Giffard, P. Alonso, J. Garín, A. Gorgues, T. P. Nguyen, P. Richomme, A. Robert, J. Roncali and S. Uriel, *Adv. Mater.* 1994, **6**, 298.

4 V. D. Sen´ and V. A. Golubev, *J. Phys. Org. Chem.* 2009, **22**, 138.

5 Octamethylbiphenylene and adamantylideneadamantane were also reported to show an electron transfer disproportionation by acids, although the phenomenon was not fully elucidated experimentally; (a) H. Hart, A. Teuerstein and M. A. Babin, *J. Am. Chem. Soc.* 1981, **103**, 903; (b) R. Rathore, C. Zhu, S. C. Lindeman and J. K. Kochi, *J. Chem. Soc., Perkin Trans. 2* 2000, 1837-1840.

6 (*a*) H. Wu, D. Zhang, L. Su, K. Ohkubo, C. Zhang, S. Ying, L. Mao, Z. Shuai, S. Fukuzumi and D. Zhu, *J. Am. Chem. Soc.* 2007, **129**, 6839; (*b*) H. Wu, D. Zhang and D. Zhu, *Tetrahedron Lett.* 2007, **48**, 8591; (*c*) H. Wu, D. Zhang, G. Zhang and D. Zhu, *J. Org. Chem.* 2008, **73**, 4271; (*d*) Y. Zeng, G. Zhang, D. Zhang and D. Zhu, *J. Org. Chem.* 2009, **74**, 4375; (*e*) L. Jia, G. Zhang, D. Zhang and D. Zhu, *Tetrahedron Lett.* 2010, **51**, 4515; (*f*) F. Sun, F. Hu, G. Zhang, Q. Zheng and D. Zhu, *J. Org. Chem.* 2011, **76**, 6883; (g) L. Tan, G. Zhang, D. Zhang and D. Zhu, *J. Org. Chem.* 2011, **76**, 9046; (*h*) L. Jia, G. Zhang, D. Zhang, J. Xiang, W. Xu and D. Zhu, *Chem. Commun.* 2011, **47**, 322; (*i*) F. Sun, F. Hu, G. Zhang and D. Zhu, *Chem. Asian J.* 2012, **7**, 183; (*j*) L. Jing, J. Guo, G. Yang, G. Zhang, C. Chen and D. Zhang, *Asian. J. Org. Chem.* 2012, **1**, 6883; (*k*) B.-T. Zhao, S.-N. Cao, H.-M. Guo and G.-R. Qu, *Synth. Met.* 2013, **174**, 14; (*l*) B.-T. Zhao, A.-M. Pen, X.-M. Zhu, Z.-N. Yan and W.-M. Zhu, *J. Org. Chem.* 2015, **80**, 1052.

7 (*a*) J.-S. Park, E. Karnas, K. Ohkubo, P. Chen, K. M. Kadish, S. Fukuzumi, C. W. Bielawski, T. W. Hudnall, V. M. Lynch and J. L. Sessler, *Science* 2010, **329**, 1324; (*b*) S. Fukuzumi, K. Ohkubo, Y. Kawashima, D. S. Kim, J. S. Park, A. Jana, V. M. Lynch, D. Kim and J. L. Sessler, *J. Am. Chem. Soc.* 2011, **133**, 15938; (*c*) S. Fukuzumi, K. Ohkubo, F. D'Souza and J. L. Sessler, *Chem. Commun.* 2012, **48**, 9785; (*d*) N. L. Bill, M. Ishida, S. Bähring, J. M. Lim, S. Lee, C. M. Davis, V. M. Lynch, K. A. Nielsen, J. O. Jeppesen, K. Ohkubo, S. Fukuzumi, D. Kim and J. L. Sessler, *J. Am. Chem. Soc.* 2013, **135**, 10852.

8 (*a*) W. M. Haynes, *CRC Handbook of Chemistry and Physics, 95th Edition*, CRC Press, Boca Rayton, 2014; (*b*) S. Dai, P. Ravi and K. C. Tam, *Soft Matter.* 2008, **4**, 435; (*c*) J. Han, K. Burgess, *Chem. Rev.* 2010, **110**, 2709; (*d*) J. Hu and S. Liu, *Macromolecules* 2010, **43**, 8315.

9 F. A. Neugebauer, H. Fischer, S. Bamberger and H. O. Smith, *Chem. Ber.* 1972, **105**, 2694.

10 S. Stoll and A. Schweiger, *J. Magn. Reson.* 2006, **178**, 42.

11 P. Job, *Ann. Chim.* 1928, **9**, 113.

12 The compounds without N-N covalent bond have two conformations (extended and folded) depending on the direction of two carbazoles or acridines. Both conformers in each compound were optimized by DFT calculation and the conformer with a lower energy is shown in Scheme 6, 7, 8 and Fig. 21, 22. See also ESI.

13 (*a*) K. Fukui, T. Yonezawa and H. Shingu, *Chem. Phys.* 1952, **20**, 722; (*b*) R. B. Woodward and R. Hoffmann, *J. Am. Chem. Soc.* 1965, **87**, 395.

14 The closed-shell singlet, the triplet, and the open-shell singlet states were calculated, giving the lowest energies for the open-shell singlet states.

15 (*a*) H. Wieland and S. Gambarjan, *Ber.* 1906, **39**, 1499; (*b*) G. S. Hammond, B. Seidel and R. Pincock, *J. Org. Chem.* 1963, **28**, 3275.

16 (*a*) F. A. Neugebauer and S. Kuhnhäuser, *Angew. Chem. Int. Ed. Engl.* 1985, **24**, 596; (*b*) M. Dietrich, J. Heinze, H. Fischer and F. A. Neugebauer, *Angew. Chem. Int. Ed. Engl.* 1986, **25**, 1021; (*c*) M. Dietrich, J. Heinze, S. Kuhnhäuser and F. A. Neugebauer, *J. Am. Chem. Soc.* 1996, **118**, 5020.

17 A. W. Franz, F. Rominger and T. J. J. Müller, *J. Org. Chem.* 2008, **73**, 1795.